

# Construction of Curcumin and Paclitaxel Co-Loaded Lipid Nano Platform and Evaluation of Its Anti-Hepatoma Activity in vitro and Pharmacokinetics in vivo

Yuxun Wei<sup>1-4,\*</sup>, Yumeng Wei<sup>1-4,\*</sup>, Lin Sheng<sup>1-4</sup>, Jingwen Ma<sup>1-4</sup>, Zhilian Su<sup>1-4</sup>, Jie Wen<sup>1-4</sup>, Lanmei Li<sup>5</sup>, Qiang Jia<sup>2,6</sup>, Huiyang Liu<sup>1-4</sup>, Hui Si<sup>2,4</sup>, Linjin Xiong<sup>1-4</sup>, Jinglin Chen<sup>1-4</sup>, Ju Cheng<sup>3,4</sup>, Ying Zuo<sup>2,7</sup>, Hongru Yang<sup>8</sup>, Ling Zhao<sup>2-4</sup>

<sup>1</sup>Key Laboratory of Medical Electrophysiology, Ministry of Education, School of Pharmacy of Southwest Medical University, Luzhou, People's Republic of China; <sup>2</sup>Key Laboratory of Medical Electrophysiology, Ministry of Education, The Affiliated Traditional Chinese Medicine Hospital of Southwest Medical University, Luzhou, Sichuan, People's Republic of China; <sup>3</sup>Central Nervous System Drug Key Laboratory of Sichuan Province, School of Pharmacy of Southwest Medical University, Luzhou, Sichuan, People's Republic of China; <sup>4</sup>Luzhou Key Laboratory of Traditional Chinese Medicine for Chronic Diseases Jointly Built by Sichuan and Chongqing, The Affiliated Traditional Chinese Medicine Hospital of Southwest Medical University, Luzhou, Sichuan, People's Republic of China; <sup>5</sup>Nanchong Key Laboratory of Individualized Drug Therapy, Department of Pharmacy, Nanchong Central Hospital, The Second Clinical Medical College, North Sichuan Medical College, Nanchong, Sichuan, People's Republic of China; <sup>6</sup>Ethics Committee Office, The Affiliated Traditional Chinese Medicine Hospital of Southwest Medical University, Luzhou, Sichuan, People's Republic of China; <sup>7</sup>Department of Comprehensive Medicine, The Affiliated Traditional Chinese Medicine Hospital of Southwest Medical University, Luzhou, Sichuan, People's Republic of China; <sup>8</sup>Department of Oncology, The Affiliated Hospital of Southwest Medical University, Luzhou, Sichuan, People's Republic of China

\*These authors contributed equally to this work

Correspondence: Ling Zhao, Key Laboratory of Medical Electrophysiology, Ministry of Education, Luzhou Key Laboratory of Traditional Chinese Medicine for Chronic Diseases Jointly Built by Sichuan and Chongqing, The Affiliated Traditional Chinese Medicine Hospital of Southwest Medical University, Luzhou, Sichuan, People's Republic of China, Tel/Fax +86 830 3160093, Email zhaoling-998@163.com; Hongru Yang, Department of Oncology, The Affiliated Hospital of Southwest Medical University, Luzhou, Sichuan, People's Republic of China, Tel/Fax +86 830 8585668, Email yanghongru801@126.com

**Purpose:** The present study aimed to construct a co-loading platform encapsulating curcumin and paclitaxel at ratios of 2:1–80:1 (w/w) designated “CU-PTX-LNP” and explored the synergistic effects of CU-PTX at different composite proportions on liver cancer cells using the combination index (CI) method.

**Methods:** The CU lipid nanoplatform (CU-LNP) formulation was optimized via single-factor and orthogonal experiments. Various concentrations of PTX were added to the optimal formulation of CU-LNP to generate CU-PTX-LNP and the nanoplatform characterized via differential scanning calorimetry (DSC), transmission electron microscope (TEM), X-ray diffraction (XRD), zeta potential, polydispersity index (PDI), and size analyses. The cumulative release, stability, and cytotoxicity of CU-PTX-LNP in LO2, HepG2, and SMMC-7221 cells were assessed in vitro, followed by safety investigation and pharmacokinetic studies in vivo. The anti-tumor activity of CU-PTX-LNP was also evaluated using nude mice.

**Results:** CU-PTX-LNP formulations containing CU:PTX at a range of proportions (2:1–80:1; w/w) appeared as uniformly dispersed nanosized spherical particles with high entrapment efficiency (EE> 90%), sustained release and long-lasting stability. Data from in vitro cytotoxicity assays showed a decrease in the IC<sub>50</sub> value of PTX of CU-PTX-LNP (by 5.47–332.7 times in HepG2 and 4.29–143.21 times in SMMC-7221 cells) compared to free PTX. In vivo, CU-PTX-LNP displayed excellent biosafety, significant anti-tumor benefits and enhanced pharmacokinetic behavior with longer mean residence time (MRT<sub>(0-t)</sub>; CU: 4.31-fold, PTX: 4.61-fold) and half-life (t<sub>1/2z</sub>; CU: 1.83-fold, PTX: 2.28-fold) relative to free drugs.

**Conclusion:** The newly designed CU-PTX-LNP platform may serve as a viable technological support system for the successful production of CU-PTX composite preparations.

**Keywords:** curcumin, paclitaxel, lipid nano platform, synergistic effect

## Introduction

Paclitaxel (PTX), a natural diterpenoid compound with anticancer activity, is a broad-spectrum clinical agent with unique antitumor mechanisms<sup>1</sup> achieved mainly through promoting microtubule formation and inhibiting microtubule depolymerization. Recent intriguing studies suggest that in addition to this classical mechanism, PTX combats cancer through multiple pathways, including regulation of immune mechanisms,<sup>2</sup> induction of apoptosis,<sup>3,4</sup> and inhibition of tumor cell migration.<sup>5</sup> However, long-term usage of PTX is significantly associated with drug resistance. Resistance of cancer cells to PTX is related to upregulation of nuclear NF- $\kappa$ B, overexpression of P-glycoprotein (P-gp) and other ABC transporters, and alterations in tubulin structures.<sup>6,7</sup> Moreover, PTX induces severe toxic reactions such as hypersensitivity,<sup>8</sup> neuromuscular toxicity,<sup>9</sup> cardiotoxicity,<sup>10</sup> and myelosuppression.<sup>11</sup> Although combination chemotherapy with cisplatin and PTX has been widely applied in the treatment of malignant tumors, this strategy has achieved limited success in effectively alleviating associated adverse effects.<sup>12</sup> Further studies are essential to target the side-effects and complications regarding drug tolerance of PTX to facilitate its clinical use.<sup>13</sup>

Over recent years, synergistic treatment of malignant tumors with PTX and natural compounds has increasingly become a research hotspot. Multitudinous preclinical studies have confirmed that combinations of PTX and natural active ingredients, in particular, curcumin (CU), present an effective strategy to reverse multiple drug resistance (MDR), reduce toxicity, and synergistically improve the efficacy of cancer therapy.<sup>14,15</sup> Notably, several studies have reported a synergistic effect of CU in combination with PTX, which may be associated with dose-dependent CU-mediated alterations in the tumor microenvironment, suppression of tumor initiation and metastasis, downregulation of P-gp, MRP-1, and ABCG2 expression to reverse MDR, and significant inhibition of NF- $\kappa$ B promoter activity.<sup>14–17</sup>

Despite its utility, the inherent characteristics of CU (poor water solubility, chemical instability, rapid metabolism through enzymes in the human body and limited bioavailability) and PTX (low water solubility and poor bioavailability) continue to pose a significant challenge for therapeutic efficacy.<sup>18–22</sup> Consequently, identification of new, effective dosage forms of the co-delivery system remains an important research focus. Numerous groups have attempted to develop nanodrug delivery systems, including micelles, polymeric nanoparticles, liposomes and solid lipid nanoparticles, in an effort to enhance the therapeutic efficacy of CU-PTX combinations and address the drug delivery issues.<sup>23–27</sup> Due to their exceptional biocompatibility, stability, safety, and modifiability, lipid nanoparticles have been researched as carriers for delivering insoluble medications like CU and/or PTX.<sup>28–30</sup> Particularly, Curcumin-human serum albumin nanoparticles decorated with programmed death ligand 1 (PDL1) binding peptide not only improve tumor-targeting drug delivery but also reestablish immune response by blocking PDL1/PD1 interaction.<sup>31</sup> Additionally, the nanodelivery systems loading CU decorated with vitamin E-tocopheryl polyethylene glycol succinate (TPGS) show noticeably improved antitumor effectiveness and the ability to favorably regulate the proteins involved in tumor development to stop tumor progression and reverse tumor immunosuppression.<sup>32</sup>

To our knowledge, the majority of research to date has focused on the possibility of combined drug delivery for cancer treatment at a relatively fixed ratio of CU:PTX.<sup>16,33–36</sup> For instance, Pi et al<sup>37</sup> prepared solid lipid nanoparticles containing PTX and CU (1:2; w/w), which increased the therapeutic impact by extending the half-life and mean residence time of the drug in vivo. In another study by Feng et al,<sup>14</sup> liposomes containing a combination of PTX and CU exerted greater cytotoxicity against A549 and A549T cells than the CU-PTX drug combination. Despite the fact that numerous prior studies have discovered excellent tumor suppression effects of CU-PTX in certain ratios combined with corresponding nano-delivery systems developed separately. However, the majority of them were created for specific drug prescriptions, which may not meet the needs of transporting different ratios of CU-PTX drug prescriptions. From the standpoint of novel research and development, a platform that can effectively transport CU and PTX at a range of proportions is urgently required to address clinical therapeutic needs. In this scenario, the study attempted to generate of a universal liposome platform that could readily and effectively encapsulate CU-PTX at a range of proportions (2:1–80:1; w/w), facilitating safer and more effective delivery. In addition, the synergistic effect was investigated in the hepatocyte model and pharmacokinetic behavior, biosafety and antineoplastic activity assessed in vivo, thus providing a platform to support the development of CU-PTX compound preparations in the clinic.

## Materials and Methods

### Materials

CU (purity  $\geq 98\%$ ) and PTX (purity  $\geq 98\%$ ) were purchased from Chengdu Best Reagent Co., Ltd (Sichuan, China). Hydrogenated soy phosphatidylcholine (HSPC) was obtained from Lipoid GmbH (Ludwigshafen, Germany), polyvinylpyrrolidone (PVP<sub>K15</sub>) from Yousuo Chemical Technology Co., Ltd (Shandong, China), and phosphoric acid (AR) from Xilong Chemical Co., Ltd (Shanghai, China). Methanol (AR), ethanol (AR), and triethylamine (AR) were purchased from Chengdu Kelong Chemical Reagent Factory (Sichuan, China). Methanol (HPLC) and acetonitrile (HPLC) were acquired from Thermo Fisher Scientific (Shanghai, China) Co., Ltd.

### Construction and Optimization of CU-PTX-LNP

A CU-PTX co-loading platform, designated CU-PTX-LNP, was constructed with the aid of ultrasonic dispersion technology. To save costs, an orthogonal test method was designed to optimize the prescription of CU-LNP after single-factor test and different amounts of PTX added to the optimal prescription to develop a co-loaded lipid nanoplat-form successfully encapsulating CU and PTX at a range of proportions. Specifically, CU, HSPC, and PVP<sub>K15</sub> were dissolved in 3 mL chloroform (CHCl<sub>3</sub>) and different amounts of PTX powder subsequently added to obtain CU:PTX mixtures at ratios of 2:1, 5:1, 10:1, 20:1, 40:1 and 80:1 (w/w; Table 1), which were dried in a rotary evaporator at 150 rpm for 15 min under vacuum. The dried lipid film was hydrated with 6 mL of 1% (w/v) sucrose aqueous solution via ultrasonic dissolving for 3 min. The mixture was emulsified via probe sonication (Ningbo Xinzhi Biotechnology co. Ltd., Zhejiang, China) for 4 min (50% ultrasonic intensity). Finally, the products were filtered using a 0.22  $\mu\text{m}$  filter membrane and freeze-dried. Dried samples were filled with N<sub>2</sub> gas and stored in a freezer at 4°C for further in vitro and in vivo study (Figure 1).

A high-performance liquid chromatography (HPLC) (Dionex, American) system fitted with the Luna C18 column (4.6 mm x 250 mm, 5  $\mu\text{m}$ ) was utilized to estimate the concentrations of CU and PTX. The mobile phase consisted of acetonitrile (A) and phosphoric acid buffer system (containing 0.01% phosphoric acid, B) with a flow rate of 1 mL/min and column temperature was maintained at 25°C. The gradient elution protocol was as follows: 0–10.2 min (55% A) and 10.21–13.2 min (40% A). Detection wavelengths were 227 nm (0–10.2 min) and 425 nm (10.21–13.2 min), respectively.

### Encapsulation Efficiency and Drug Loading

Due to their extremely poor water solubility, free PTX and CU drugs typically precipitate in water while liposomes with small particle sizes are not precipitated under low- or medium-speed centrifugation. In our experiments, low-speed centrifugation was employed for separation. Encapsulation efficiency (EE) and drug Loading efficiency (DL) of PTX and CU were determined using the HPLC system based on a previous analytical protocol. For determination of EE, the amounts of CU and PTX were measured in the same quantity of liposome suspension before and after low-speed centrifugation (8000 rpm, 10 min), which was diluted with methanol and sonicated (200 W, 40 kHz, 5 min) to ensure complete drug release.

For assessment of DL, a specific amount of freeze-dried nanoparticles was accurately weighed, diluted with an appropriate amount of methanol, and demulsified via ultrasonic irradiation (200 W, 40 kHz, 5 min). The CU and PTX contents were determined via HPLC after filtration. EE and DL values were calculated as follows:

**Table 1** Different Proportions of the Formula

No.	Formulations	CU (mg)	PTX (mg)	PVP <sub>K15</sub> (mg)	HSPC (mg)
1	CU-PTX-LNP (2:1)	5	2.5	8	70
2	CU-PTX-LNP (5:1)	5	1	8	70
3	CU-PTX-LNP (10:1)	5	0.5	8	70
4	CU-PTX-LNP (20:1)	5	0.25	8	70
5	CU-PTX-LNP (40:1)	5	0.125	8	70
6	CU-PTX-LNP (80:1)	5	0.0625	8	70

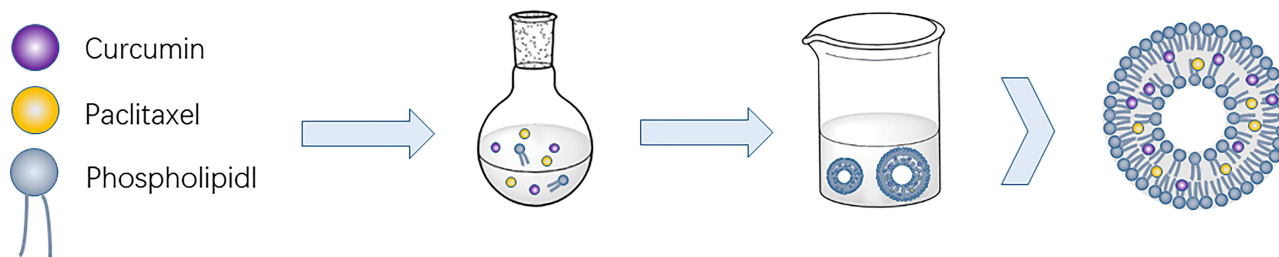


**Figure 1** Assembly diagram of CU-PTX-LNP.

$$EE(\%) = \frac{W_{\text{incorporated}}}{W_{\text{total}}} \times 100\%$$

$$DL(\%) = \frac{W_{\text{total}}}{W_{\text{lipids}}} \times 100\%$$

where  $W_{\text{incorporated}}$  is the weight of drug encapsulated in liposomes,  $W_{\text{total}}$  the total amount of drug in the formulation, and  $W_{\text{lipids}}$  the total weight of lipids.

## Characterization of CU-PTX-LNP

### Size and Zeta Potential

To generate a lipid nanometer solution, a suitable quantity of lyophilized powder was dissolved in an amount of distilled water. Marvin laser granulometry was applied to assess particle size, electrical properties (zeta potential), and PDI.

### TEM

CU-PTX-LNP lyophilized powder was diluted with an appropriate quantity of water at room temperature. After staining with phosphotungstic acid solution, a tiny drop of the sample was placed carefully on a copper grid, vacuum-dried, and examined via transmission electron microscopy.

### DSC

CU, PTX, blank LNP lyophilized powder and CU-PTX-LNP lyophilized powder were precisely weighed and placed in an aluminum sample pan for pressing. An empty aluminum container was used as the reference cell. The heating range was 35–500°C and heating rate was 10°C/min with nitrogen as the carrier gas. The above four samples were scanned.

### XRD

CU, PTX, blank LNP lyophilized and CU-PTX-LNP lyophilized powder samples were analyzed with XRD (D8 ADVANCE X-ray diffractometer; Bruker, Germany) under the following conditions: Cu target wavelength: 1.5406 Å, Co target wavelength: 1.79026 Å, voltage: 40 kV, current: 40 mA, diffraction angle ( $2\theta$ ) scanning range: 10°–90°, scanning speed: 6°/min.

## Cell Lines and Cultures

HepG2, SMMC-7721 and LO2 cell lines (Chinese Academy of Sciences Cell Bank) were cultured in RPMI or DMEM supplemented with heat-inactivated fetal bovine serum (FBS) (10%), penicillin (100 U/mL), and streptomycin (100 µg/mL). Cultures were incubated at 37°C in a humidified atmosphere containing 5% CO<sub>2</sub>. Cells in the exponential growth phase were used for experiments.

## Cell Cytotoxicity Assay

Cells in the logarithmic growth phase were cultured in 96-well plates at a density of  $5 \times 10^3$  cells per well. After incubation of cultures for 24 h, different concentrations of drugs were dispersed in RPMI or DMEM and 200 µL drug solution added to each well. Following 48 h of cell culture, MTT solution was added to each well and incubated for 3.5 h. The liquid



supernatant was discarded, 200  $\mu$ L DMSO added and the mixtures shaken for 15 min. Cells incubated in wells without drugs were used as the control group. Absorbance (A) of each well was measured at 490 nm using an enzyme label analyzer. The inhibition rate of cell proliferation was calculated as follows:

$$\text{Inhibition rate} = 1 - \frac{A_{\text{drug group}} - A_{\text{blank group}}}{A_{\text{control group}} - A_{\text{blank group}}} \times 100\%$$

## Synergy Index of CU and PTX Combinations at Various Ratios

The median-effect principle was applied to determine the nature of action of the drug combination.<sup>38</sup> Before examination of the combination effect, we plotted the dose-effect curves of the two drugs when applied alone and in combination. The synergistic index of the two drugs at different inhibition rates was calculated using the following median effect equation:

$$CI = \frac{(D)_1}{(D_x)_1} + \frac{(D)_2}{(D_x)_2} + a \frac{(D)_1(D)_2}{(D_x)_1(D_x)_2}$$

where  $(D_x)_1$  and  $(D_x)_2$  represent the concentrations required to produce a cell proliferation inhibition rate of x% when the two drugs are applied individually and  $(D)_1$  and  $(D)_2$  are the respective concentrations of the two drugs upon combination to produce the same x% cell proliferation inhibition rate. Combination index (CI) < 1 indicates synergism, CI = 1 summation and CI > 1 antagonism of the two drugs.  $(D_x)_1$  and  $(D_x)_2$  values were obtained using the formula:

$$D_x = D_m [f_a / (1 - f_a)]^{1/m}$$

whereby  $D_m$  is the median-effect dose,  $f_a$  the fraction affected, and m the slope of the median-effect plot.

## Evaluation of Long-Term Stability

Freeze-dried CU-PTX-LNP (2:1 and 10:1) powder prepared according to the optimized protocol was stored at a temperature of  $4 \pm 2^\circ\text{C}$  and sealed away from light. At the end of 1, 2, and 3 months, the powder was dissolved in an appropriate amount of pure water for measurement of EE and particle size and morphological examination.

## In vitro Release of CU-PTX-LNP

In vitro release of nanoparticles was conducted via dialysis. Briefly, an appropriate amount of CU-PTX-LNP was placed into a dialysis bag (8000–14,000 Da) in 100 mL normal saline containing 15% ethanol and 0.2% Tween 80 at  $37^\circ\text{C}$ . At the appropriate time intervals, sample aliquots (1 mL) were withdrawn from the release medium and filtered through a 0.22  $\mu\text{m}$  membrane filter. An equivalent volume of blank dissolution medium at the same temperature was replenished to maintain the original volume after each sampling. PTX and CU concentrations in medium were measured via HPLC as described earlier.

## Safety Evaluation

### In vitro Hemolytic Analysis

Blood (10 mL) was obtained from healthy rabbits and fibrinogen removed by stirring slowly with a glass rod to form defibrinated blood. Sodium chloride solution (0.9%, 100 mL) was added to defibrinated blood and centrifuged at 1500 rpm for 10 min to remove the supernatant. Precipitated red blood cells were washed with 0.9% sodium chloride solution using the above method until the color of the supernatant was not red. Subsequently, red blood cells were prepared as a 2% suspension with 0.9% sodium chloride solution. A solution of CU (2 mg/mL) and PTX (1 mg/mL) was additionally prepared. Hematocyte suspension (2%), 0.9% sodium chloride solution, ultrapure water, and sample solution were added into the experimental tube in sequence (Table 2). Solution tubes No.1–5 were the nanometer samples, No.6 the negative control, No.7 the positive control and No.8 the reference owing to the yellow appearance of the prepared nanoparticles. The mixture was immediately incubated at  $37 \pm 0.5^\circ\text{C}$  for 1 h and centrifuged at 1500 rpm for 10 min. The supernatant (100  $\mu$ L) was transferred to a 96-well plate and absorbance determined using an enzyme microplate reader at a wavelength of 540 nm.

**Table 2** Hemolysis Test Scheme

Number of Test Tube	CU-PTX-LNP (2:1) (mL)	0.9% Saline (mL)	Ultrapure Water (mL)	2% Hematocyte (mL)
1	0.1	2.4	0	2.5
2	0.2	2.3	0	2.5
3	0.3	2.2	0	2.5
4	0.4	2.1	0	2.5
5	0.5	2.0	0	2.5
6	0	2.5	0	2.5
7	0	0	2.5	2.5
8	0.5	2.0	0	0

### In vivo Acute Toxicity

Newly purchased Kunming mice (KM; weight:  $30 \pm 2$  g) were randomly divided into 6 groups (n=6 per group). The following groups were given intraperitoneal injections (injection volume: 0.3 mL): Control group (saline), CU group (dose: 60 mg/kg), PTX group (dose: 30 mg/kg), CU-PTX group (dose: CU: 60 mg/kg; PTX: 30 mg/kg), CU-PTX-LNP group (dose: CU: 360 mg/kg; PTX: 180 mg/kg), LNP group (dose: same as CU-PTX-LNP group equivalent). After administration, the mice were observed for their daily diet and mental status. On the 8th day of the experiment, all mice were executed, and three mice in each group were randomly selected to collect blood samples and test the biochemical parameters (ALT, AST, ALP, CREA, UA and UREA) reflecting liver and kidney function. Hematoxylin and eosin (HE) staining of the heart, liver, and kidney tissues of dissected mice allowed for pathological section analysis.

### Pharmacokinetic Studies

All in vivo experimental protocols were approved by the Animal Care Committee of Southwest Medical University. Experiments were carried out in strict accordance with the guidelines of laboratory animal care adopted by the National Institutes of Health (Shanghai, China). Twelve clean-grade rabbits (1.0–1.5 kg) from the Animal Center of Southwest Medical University (license number for animal use: SYXK (Sichuan) 2018–065) were employed to study the effects of the combined drugs on pharmacokinetics. After adaptive rearing for one week, rabbits were randomly divided into two groups (6 animals per group) subjected to either intravenous injection of free CU-PTX (A) or CU-PTX-LNP (B). All animals were maintained in a state of fasting for 12 h before the experiment. The doses of CU and PTX used were 16 mg/kg and 8 mg/kg and free drug suspensions were prepared with ethanol-hydrogenated castor oil (1:1, v/v). Blood samples were collected into heparinized 1.5 mL polythene tubes at 5, 10, 15, 30, 45, 60, 120, 240, 360, 480, 720, and 1440 min after dosing. Samples were immediately centrifuged for 3 min (5000 rpm) and the supernatant fractions (500  $\mu$ L) transferred to a 10 mL centrifuge tube for further analysis.

### In vivo Antitumor Assessment

First, 100  $\mu$ L of tumor cell suspension ( $3 \times 10^7$  cells/mL) was inoculated into the left axilla of BALB/C nude mice. Then, the tumor-bearing nude mice were split into groups at random (n=6 per group). The medication intervention was started after the tumors reached a volume of approximately 100 mm<sup>3</sup>. The tumor-bearing nude mice received intraperitoneal injections of the following substances: (1) saline (Control group), (2) CU (16 mg/kg), (3) PTX (8 mg/kg), (4) CU-PTX (16 mg/kg CU; 8 mg/kg PTX;), (5) CU-PTX-LNP (16 mg/kg CU; 8 mg/kg PTX). Intraperitoneal injections were given to all groups every three days for 14 days. The body weight and tumor volume of all tumor-bearing nude mice were measured every 2 days. At the end of the administration, the nude mice were euthanized and the tumors were excised and weighed.

## Statistical Analysis

All data were obtained using the SPSS 17.0 statistical package. Data were expressed as mean  $\pm$  standard deviation (SD) in triplicate. Differences among multiple groups were determined using Student's *t*-test or one-way ANOVA with a post-hoc test and considered statistically significant at  $P < 0.05$ .

## Results and Discussion

### Construction and Optimization of CU-PTX-LNP

For cost saving purposes, single-factor investigations and optimization of the CU-LNP formulation were initially conducted. As shown in Figure 2, the preparation process (sonication temperature, sonication time and sonication intensity) of CU-LNP was optimized based on single factors. We observed an increase in EE and decrease in particle size with increasing temperatures (25–45°C). With increasing sonication times (5–10 min), particle size and PDI decreased and EE initially increased and subsequently decreased. After 7–10 min, we observed no significant differences in particle size, PDI or EE. In the range of 40–70%, EE reached maximum value at 50% ultrasonic intensity. Accordingly, the tentative optimal preparation process of CU-LNP was set at a rotary evaporation temperature of 45°C, probe ultrasonic time of 7 min and ultrasonic intensity of 50%.

Taking the parameters EE, DL, and PDI as the inspection indicators, after comprehensive evaluation, the optimal doses of the main drugs (CU, PVP<sub>K15</sub>, and HSPC) were tentatively determined as 5, 10, and 60 mg, respectively. CU-LNP prepared under these conditions showed EE of  $95.61 \pm 0.82\%$ , DL of  $3.39 \pm 0.30\%$  and PDI of  $0.179 \pm 0.055$ . Sucrose was selected as the freeze-drying protective agent and the properties of CU-LNP before and after freeze-drying investigated based on particle size and PDI as indicators. Changes in particle size and PDI before and after lyophilization were minimal with the addition of 1% sucrose, which was thus selected as the cryoprotectant.

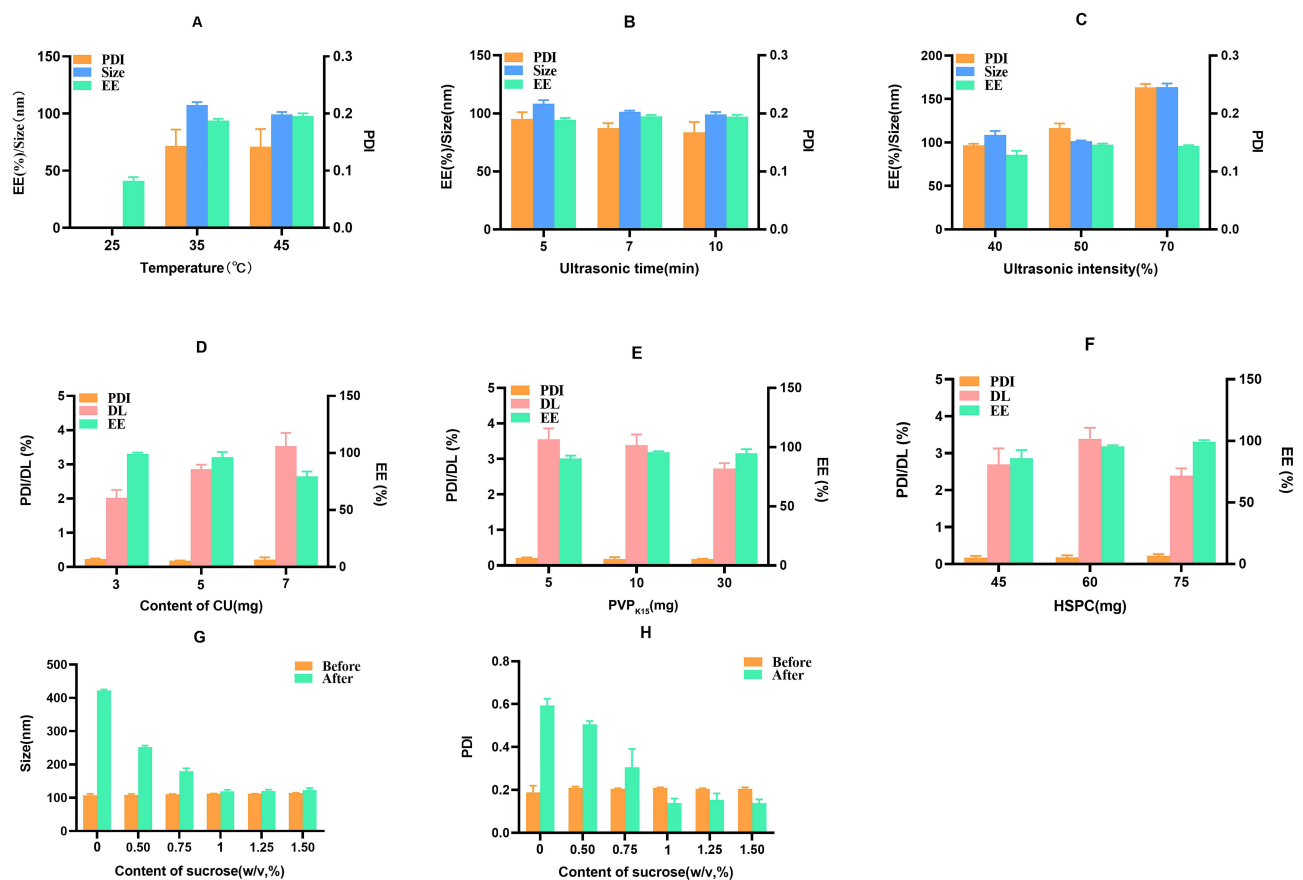


**Figure 2** Single factor inspection. Influence of temperature (A), ultrasonic time (B), and ultrasonic intensity (C) on the EE, particle size, and PDI of CU-LNP. Influence of CU (D), PVP<sub>K15</sub> (E), and HSPC (F) on the EE, DL, and PDI of CU-LNP. Influence on particle size (G) and PDI (H) of CU-LNP by cryoprotectants.

On the basis of single-factor tests, three main factors affecting CU-LNP quality were identified, specifically, amounts of CU (A), HSPC (B), and PVP<sub>K15</sub> (C). Comprehensive L9 (3<sup>3</sup>) design experiments were conducted and nine prescriptions determined. The formulations and results of EE, DL, and PDI determinations are shown in Table 3. Comparison of the effects of the three factors on EE, DL, and PDI via analysis of variance (Table 4) revealed that HSPC and CU contents had a significant influence ( $P < 0.05$ ). The optimal proportions of CU, HSPC, and PVP<sub>K15</sub> in the formulation were determined as A<sub>3</sub>B<sub>3</sub>C<sub>2</sub>.

Three batches of different proportions of CU-PTX-LNP were generated using the optimized formulation and preparation process. The particle sizes, PDI, and zeta potential of the different CU-PTX-LNP combinations are presented in Table 5. The hydrodynamic sizes of CU-PTX-LNP synthesized in this study were 90–120 nm, which is within the optimal range for cellular uptake.<sup>39</sup> Consequently, due to enhanced permeability and retention effects, these particles are easily able to aggregate in areas of tumor vasculature and passively target the tumor.<sup>40,41</sup> Moreover, slight changes in nanoparticle size are reported to significantly affect drug release, in vivo biodistribution, and pharmacokinetics.<sup>42–44</sup> For instance, Zhao et al<sup>45</sup> showed that 100 nm NPs exhibit better pharmacokinetic efficacy than 500 nm NPs. Additionally, the renal filtration effect is a crucial component of blood purification. Nanoscale drug carriers bigger than 20 nm typically

**Table 3** L9 (3<sup>3</sup>) Orthogonal Design Table

No.	Factors						EE (%)	DL (%)	PDI	Y
	A		B		C		Y <sub>1</sub>	Y <sub>2</sub>	Y <sub>3</sub>	
1	3	(1)	50	(1)	6	(1)	82.82	1.95	0.226	84.73
2	3	(1)	60	(2)	8	(2)	92.81	1.92	0.241	92.86
3	3	(1)	70	(3)	10	(3)	95.05	1.55	0.211	94.54
4	4	(2)	50	(1)	8	(2)	83.38	1.90	0.260	84.60
5	4	(2)	60	(2)	10	(3)	89.51	2.14	0.231	90.62
6	4	(2)	70	(3)	6	(1)	91.99	2.12	0.212	92.95
7	5	(3)	50	(1)	10	(3)	86.15	2.37	0.325	86.77
8	5	(3)	60	(2)	6	(1)	92.06	2.32	0.214	93.32
9	5	(3)	70	(3)	8	(2)	95.57	2.62	0.234	96.51

**Table 4** Analysis of Variance in Orthogonal Test

No.	Sum of Squares of Deviations	Mean Square	Free Degree	F value	P
A	11.859	5.929	2	119.542	0.008
B	139.86	69.93	2	1409.879	0.001
C	1.539	0.769	2	15.51	0.061

**Table 5** The Formulation of CU-PTX-LNP

F	EE %		Size (nm)	PDI	Zeta Potential
	CU	PTX			
2:1	94.29 ± 3.61	92.73 ± 4.81	112.4 ± 6.90	0.224 ± 0.02	15.5 ± 0.50
5:1	95.84 ± 2.28	93.25 ± 2.46	105.9 ± 1.50	0.207 ± 0.03	15.5 ± 1.10
10:1	96.75 ± 1.87	95.42 ± 2.40	94.3 ± 4.80	0.247 ± 0.04	19.9 ± 1.90
20:1	97.41 ± 0.75	94.57 ± 3.55	94.3 ± 3.60	0.244 ± 0.04	18.7 ± 0.30
40:1	96.31 ± 1.90	98.64 ± 3.20	111.9 ± 2.90	0.197 ± 0.04	13.6 ± 0.20
80:1	97.44 ± 0.41	99.78 ± 3.40	108.7 ± 7.60	0.203 ± 0.03	16.8 ± 0.90

**Abbreviation:** F, Formulation.

prevent rapid urine leakage, while those smaller than 200 nm avoid macrophage capture in the reticuloendothelial system (liver and spleen).<sup>46,47</sup>

The PDI of all CU-PTX-LNPs was  $<0.3$ , indicating a uniform size distribution favorable for drug delivery systems. Small sizes and uniform distribution of liposomes ( $< 200$  nm) facilitate efficient internalization into tumor cells.<sup>48</sup> Moreover, the zeta potential of liposomes was positive. Positively charged nanoparticles effectively bind the surface of cancer cells to exert therapeutic effects, leading to inhibition of malignant cell growth.<sup>45,49</sup> EE of CU-PTX-LNP (different proportions) was  $>90\%$ . The collective data indicate that the lipid platform constructed with this preparation method successfully encapsulates CU and PTX at a range of proportions (between 2:1 and 80:1), supporting its utility as a universal carrier that can satisfy the combination drug requirements for a wide range of clinical applications.

## Characterization of CU-PTX-LNP

### TEM

Transmission electron microscopy was employed to characterize the morphology and dispersion of drug-loaded liposome platforms. The results showed an irregular spherical shape with uniform internal distribution and good dispersion (Figure 3A).

### DSC

The polymorphs, transition states, and recrystallization behavior of colloidal lipid nanoparticle-loaded systems can be effectively determined by measuring the melting point and energy changes during phase transition with the aid of DSC. Accordingly, we evaluated the melting behavior of liposomes and the physical states of constituent CU and PTX. The phase transition peak of CU appeared at  $\sim 185^{\circ}\text{C}$  and that of PTX at  $\sim 220^{\circ}\text{C}$  (Figure 3B). The curves of CU-PTX-LNP and blank LNP almost overlapped and phase transition peaks of CU and PTX disappeared, indicating that CU and PTX exist in an amorphous state in the hydrophobic core of liposome platforms.

### XRD

As shown in Figure 3C, CU and PTX displayed sharp diffraction peaks, suggestive of a crystalline state. CU displayed pronounced characteristic diffraction peaks in the range of  $10^{\circ}$ – $50^{\circ}$  and PTX in the field of  $10^{\circ}$ – $30^{\circ}$ . Both CU-PTX-LNP and blank LNP displayed smooth diffraction peaks at around  $21^{\circ}$  and the characteristic diffraction peaks of CU and PTX disappeared, indicating successful encapsulation of CU and PTX in liposome platforms. The hydrophobic inner core existed in an amorphous state, consistent with the results obtained with DSC.

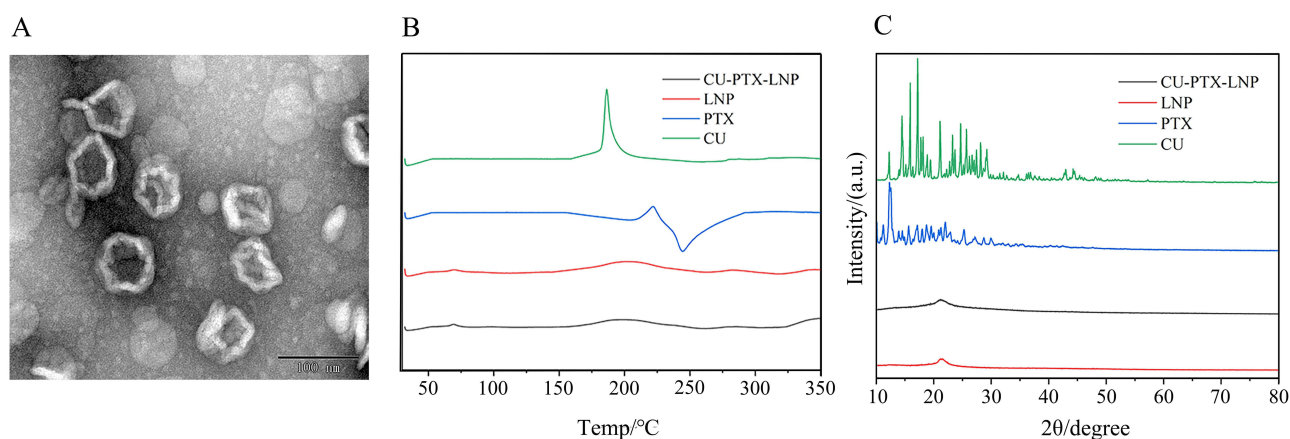


**Figure 3** Characterization of CU-PTX-LNP. (A) TEM image of CU-PTX-LNP (scale bar: 100 nm). (B) DSC pattern of CU, PTX, LNP, and CU-PTX-LNP. (C) XRD pattern of CU, PTX, LNP, and CU-PTX-LNP.



## Synergistic Effects of CU-PTX-LNP

This research further evaluated the *in vitro* drug safety and antitumor efficacy of free drugs and combination regimens using drug-sensitive cancer cell lines (Figures 4–7). The cytotoxicities of free CU, PTX and CU-PTX solution, blank liposome, and CU-PTX-LNP suspension against LO2, HepG2, and SMMC-7721 cells were measured, with 0.5% DMSO as the control. As expected, treatment with 0.5% DMSO or blank liposomes (control groups) had no significant effects on viability of the three cell lines (data not shown).

LO2, HepG2, and SMMC-7721 cells were exposed to solutions of free CU, PTX, different ratios of CU-PTX and CU-PTX-LNP suspension for 48 h. According to the intervention effect of drugs on LO2 cells, the toxicity of different groups of drugs to normal human cells can be preliminarily speculated. The IC<sub>50</sub> values of free PTX and CU solutions for LO2 were 11.39 ± 0.56 and 54.00 ± 1.99 µg/mL, respectively. As shown in Figures 4, 7A1 and A2, the IC<sub>50</sub> values of CU-PTX-LNP for LO2 were all higher (except at ratios of 2:1 and 5:1) compared to free CU solution, indicating lower cytotoxicity of the CU-PTX-LNP platform (at ratios of 10:1, 20:1, 40:1, and 80:1). Heger et al<sup>50</sup> reported high safety of CU as a food additive with no apparent side-effects, even at a dose of 12 g/d. In view of these findings, it is reasonable to speculate that the CU-PTX-LNP formulation (10:1, 20:1, 40:1, and 80:1) has a relatively high safety performance.

To determine the inhibitory effects of CU and PTX in the free and liposomal vesicle forms on HepG2 and SMMC-7721 hepatoma cells, dose-response experiments were initially conducted. Following intervention for 48 h, individual treatments resulted in inhibition of HepG2 and SMMC-7721 cell growth in a dose-dependent manner, as shown in Figures 5 and 6. In addition, both cell lines showed higher sensitivity to the formulation at different combination ratios compared with free drugs at the same concentrations. As depicted in (Figure 7B1 and C1), the IC<sub>50</sub> value of free PTX was higher than different proportions of CU-PTX in both HepG2 (2:1, 5:1, 10:1, 20:1, 40:1, 80:1) and SMMC-7721 (2:1, 10:1, 20:1, 40:1) by 4.29 to 332.7 folds. The CU-PTX combination at specific ratios (2:1, 40:1, 80:1 in HepG2 and 2:1, 10:1, 20:1, 40:1 in SMMC-7721) showed lower IC<sub>50</sub> values than free CU solution (Figure 7B2 and C2). These data indicate that combination of CU and PTX can effectively enhance the inhibitory effects of free CU and PTX solutions in HepG2 and SMMC-7721 cells. Based on considerable previous research, it is reasonable to speculate that this finding is related to CU-induced transformation of the tumor microenvironment, suppression of the occurrence and metastasis of tumors, downregulation of P-gp expression, and marked inhibition of NF-κB in a dose-dependent manner.<sup>14–16</sup> In addition, the IC<sub>50</sub> values of all CU-PTX-LNP groups were lower (1.47–6.99 folds) than the CU-PTX groups among

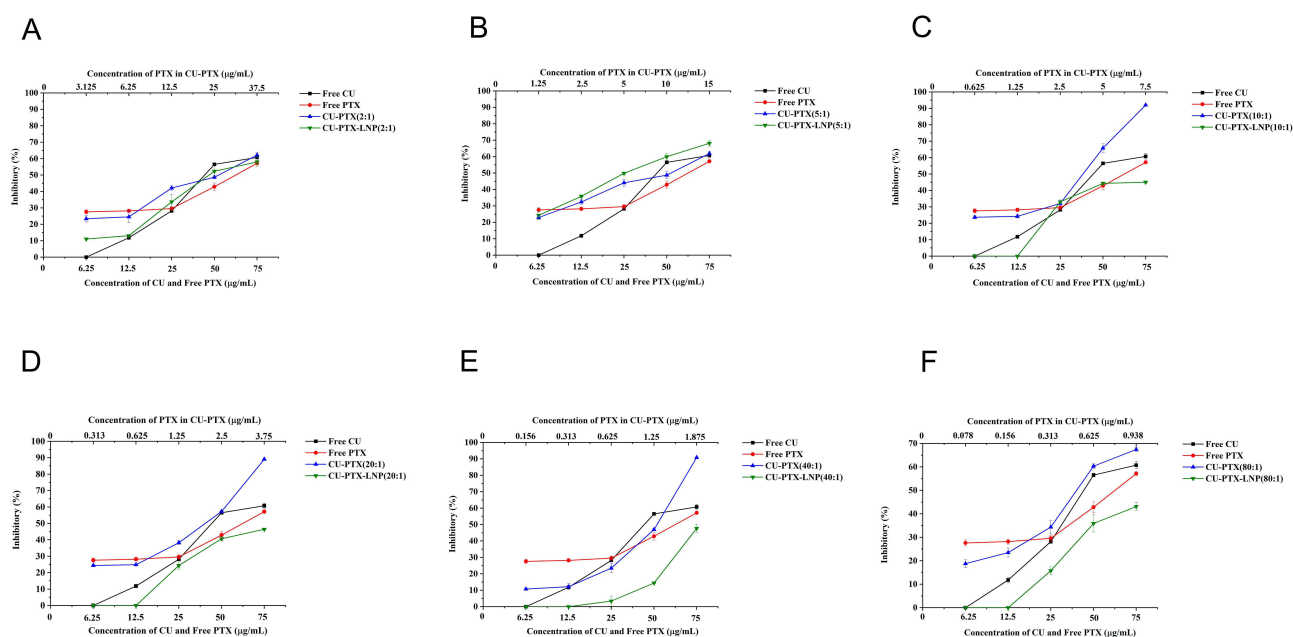


**Figure 4** Inhibition rate (%) of CU, PTX, and different ratios of CU-PTX and CU-PTX-LNP to LO2 at 48 h. (A) CU:PTX=2:1; (B) CU:PTX=5:1; (C) CU:PTX=10:1; (D) CU:PTX=20:1; (E) CU:PTX=40:1; (F) CU:PTX=80:1.

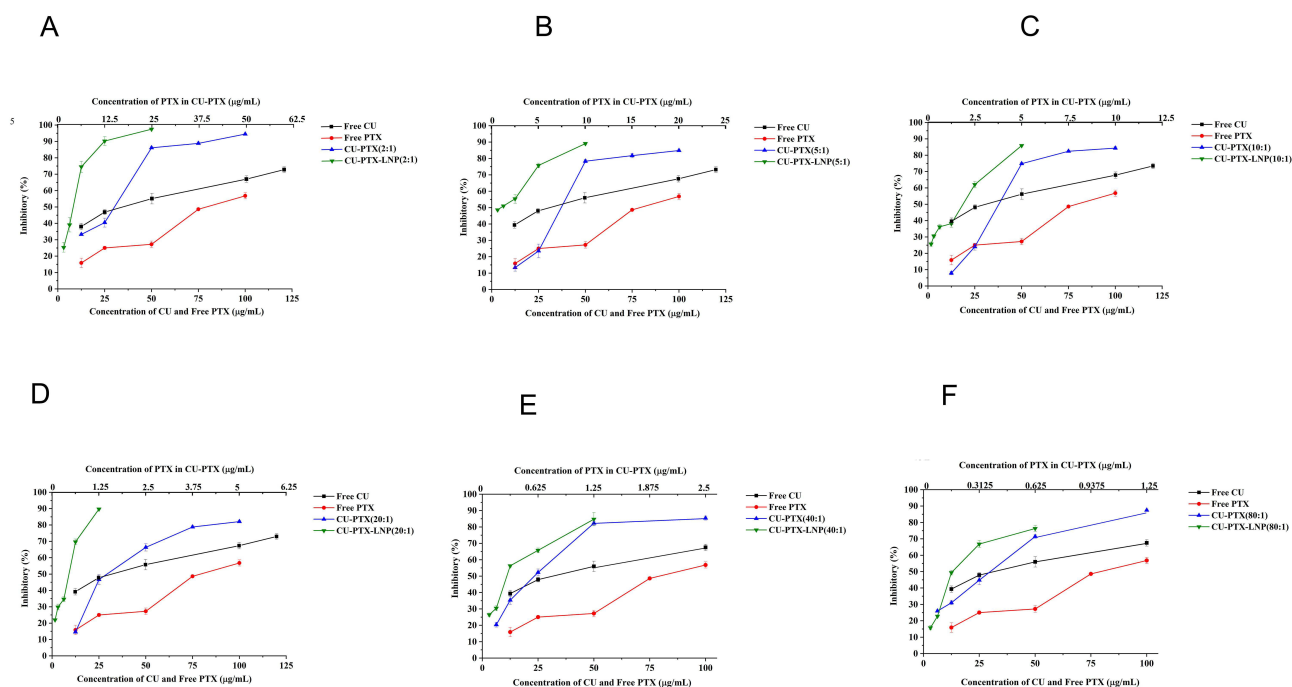


**Figure 5** Inhibition rate (%) of CU, PTX, and different ratios of CU-PTX and CU-PTX-LNP to HepG2 at 48 h. **(A)** CU:PTX=2:1; **(B)** CU:PTX=5:1; **(C)** CU:PTX=10:1; **(D)** CU:PTX=20:1; **(E)** CU:PTX=40:1; **(F)** CU:PTX=80:1.

the six combination regimens, signifying better concentration-dependent cytotoxicity ( $P < 0.05$ ). These findings indicate that our preparations of nanoliposomes effectively optimized the cancer cell killing efficiency of CU-PTX groups. The known mechanisms of particle uptake include phagocytosis, liquid-phase endocytosis, and receptor-mediated endocytosis. The primary internalization mechanism for particles 100 nm in size is endocytosis, supporting liposome distribution into the cytoplasm and nucleus. Liposomes with particle sizes smaller than 200 nm are efficiently internalized into tumor cells,<sup>51</sup> which could explain why the CU-PTX preparations generally exerted a more substantial inhibitory effect on liver cancer cells. Overall, the  $IC_{50}$  values for HepG2 and SMMC-7721 cells of the different treatment groups were in the following order: CU-PTX-LNP < CU-PTX < CU < PTX.

For further clarification of the combined effects of the two drugs, the median-effect method was utilized. As shown in Figure 7B, CI values of different proportions of CU-PTX were <1 in HepG2 and SMMC-7721 cells, indicating that combined administration of CU and PTX exerts a synergistic effect. Surprisingly, CI of CU-PTX-LNP in all groups was <0.5, which was lower than that of CU-PTX at the same proportion, suggesting that the liposome platform substantially enhanced the inhibitory effect of CU-PTX on liver cancer cell growth. The CI values of CU-PTX (<0.6) and CU-PTX-LNP (<0.4) were lower in HepG2 cells.

## Long-Term Stability

Particle size and PDI of freeze-dried CU-PTX-LNP (2:1) and CU-PTX-LNP (10:1) were determined as  $110.5 \pm 4.1$  nm,  $0.220 \pm 0.021$  and  $96.8 \pm 0.5$  nm,  $0.174 \pm 0.011$ , while EE of CU and PTX were  $95.99 \pm 3.98\%$ ,  $95.76 \pm 3.55\%$  and  $96.19 \pm 4.16\%$ ,  $94.79 \pm 3.42\%$ , respectively (Table 6 and 7). Following storage in a sealed and dark place at  $4^{\circ}\text{C}$  for 2 months, particle size and PDI of the two LNPs were  $162.1 \pm 5.1$  nm,  $0.285 \pm 0.026$  and  $100.7 \pm 0.7$  nm,  $0.146 \pm 0.012$ , while EE of CU and PTX were  $95.36 \pm 3.48\%$ ,  $94.16 \pm 3.57\%$  and  $93.45 \pm 4.40\%$ ,  $94.46 \pm 2.77\%$ , respectively. Under conditions of sealing and storage at  $4^{\circ}\text{C}$  in the dark, lyophilized liposome powder appeared loose and uniform yellow in color with a slight increase in particle size. However, EE and PDI values were not significantly changed over the storage period. These findings indicate that CU-PTX-LNP preparations at different drug ratios could be stably stored for at least two months under the above conditions.

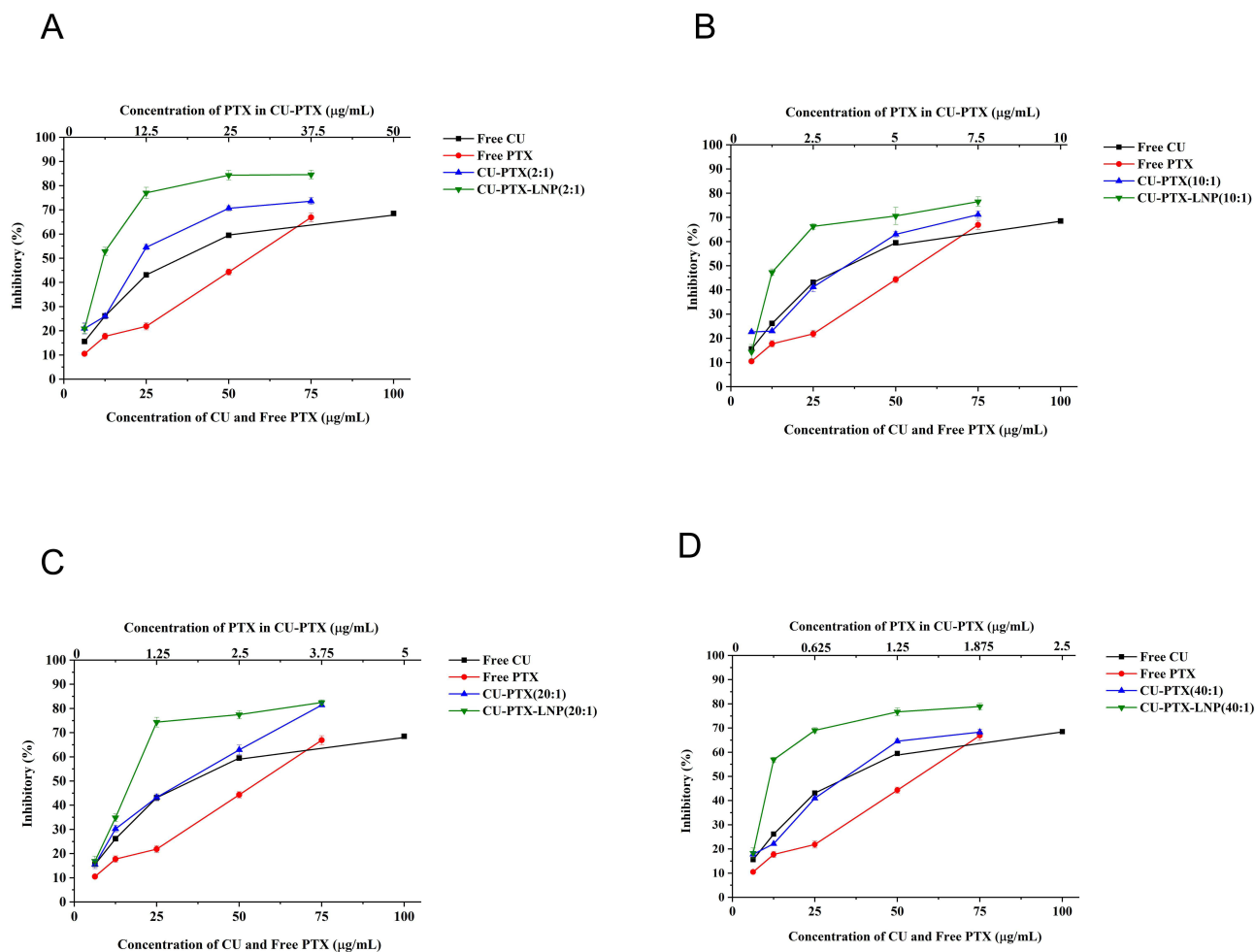


**Figure 6** Inhibition rate (%) of CU, PTX, and different ratios of CU-PTX and CU-PTX-LNP to SMMC-7721 at 48 h. (A) CU:PTX=2:1; (B) CU:PTX=10:1; (C) CU:PTX=20:1; (D) CU:PTX=40:1.

## In vitro Release

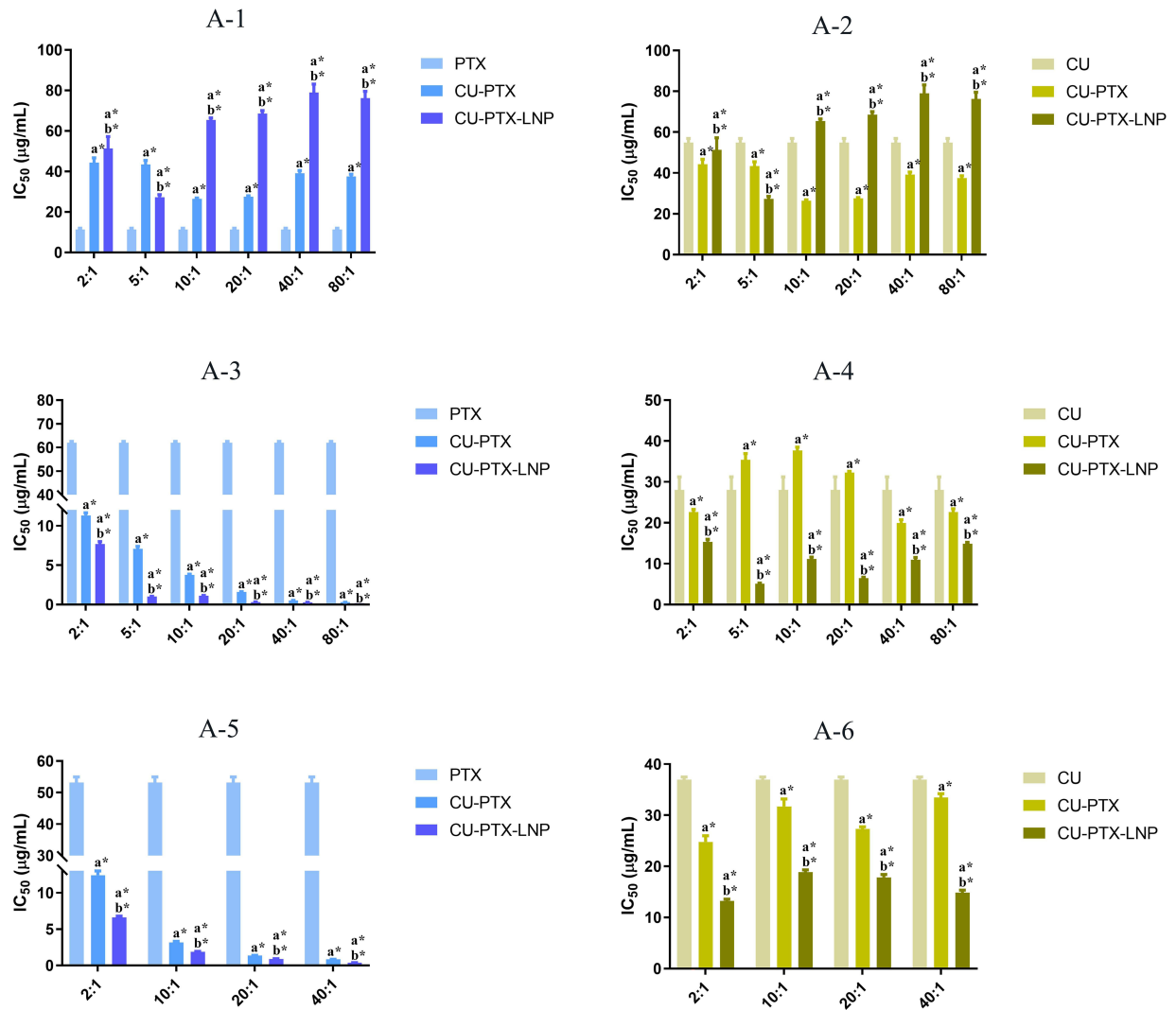
Cumulative release of CU-PTX-LNP (2:1) for 96 h in vitro is depicted in Figure 8. Data from the chart show that the release amount of CU gradually increased, with a cumulative release amount of about 60% within 96 h. Over this time period, release of PTX also steadily accelerated, with an incremental release of up to 90%. The cumulative release rate of CU-PTX-LNP was mathematically fitted to zero-order, first-order and Higuchi equations, and the correlation coefficient R calculated. A closer value of R to 1 indicates greater consistency with the release equation. A specific correlation between the release degree and time was observed using the above models (Table 8). In vitro release of CU-PTX-LNP was predominantly in line with the Higuchi release equation, one of the primary modes of sustained-release preparations, signifying that the release mechanism of nanoparticles was mainly diffusion. The results suggest that CU-PTX-LNP prepared using this method shows satisfactory behavior with no sudden release phenomenon, leading to slow and effective release of the drug.

## Safety Evaluation

### Hemolytic Test in vitro

As shown in Table 9 and Figure 9, the sample in Tube 6 (negative control) did not show hemolysis while that in Tube 7 displayed 100% hemolysis. In Tubes 1–5, erythrocytes were deposited at the bottom of the test tube with no evidence of prominent hemolysis. This phenomenon occurs because erythrocytes do not hemolyze under normal conditions while

A



B

Prescription	CI at Fa=0.75					
	2:1	5:1	10:1	20:1	40:1	80:1
CU-PTX	0.526	0.5469	0.4697	0.4471	0.3055	0.3535
CU-PTX-LNP	0.3925	0.1849	0.3169	0.0962	0.2005	0.2501

Prescription	CI at Fa=0.75			
	2:1	10:1	20:1	40:1
CU-PTX	0.8963	0.8873	0.5679	0.8108
CU-PTX-LNP	0.3796	0.4784	0.3595	0.371

**Figure 7 (A)** IC<sub>50</sub> values of PTX, CU, and different ratios of CU-PTX and CU-PTX-LNP on LO2 (PTX: A-1; CU: A-2), HepG2 (PTX: A-3; CU: A-4), and SMMC-7721 (PTX: A-5; CU: A-6) cells at 48h. **(B)** CI of CU-PTX and CU-PTX-LNP at different groups to HepG2 cells (B-1) and SMMC-7721 cells (B-2).

**Notes:** P <0.05, there was a significant difference compared with PTX or CU solution (a\*), or the same drug proportion of CU-PTX (b\*).

**Abbreviation:** Fa, Fraction affected.

severe hemolysis occurs in hypotonic medium. The highest hemolysis rate of each lipid nanoparticle was 3.17 ± 0.56%, supporting the biocompatibility of LNPs prepared in this experiment.

### In vivo Acute Toxicity

Mice in the PTX group started exhibiting negative clinical symptoms such as unstable gait, impaired mobility, and lowering body temperature right away after injection. All mice in this group perished one by one within 6 h, and the first

**Table 6** Stability of the CU-PTX-LNP (2:1) Freeze-Dried Powder

Time(Month)	EE (%)		Size (nm)	PDI
	CU	PTX		
0	95.99 ± 3.98	95.76 ± 3.55	110.5 ± 4.1	0.220 ± 0.021
1	95.89 ± 0.95 <sup>#</sup>	95.78 ± 5.03 <sup>#</sup>	141.0 ± 11.0	0.219 ± 0.027 <sup>#</sup>
2	95.36 ± 3.48 <sup>#</sup>	94.16 ± 3.57 <sup>#</sup>	162.1 ± 5.1	0.285 ± 0.026 <sup>#</sup>
3	82.72 ± 6.91	78.73 ± 4.39	183.6 ± 6.1	0.372 ± 0.032

Note: <sup>#</sup>Compared with month 0, P >0.05.

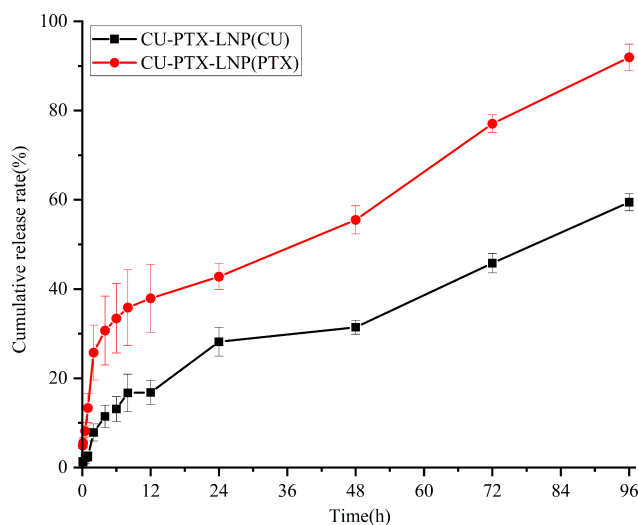
**Table 7** Stability of CU-PTX-LNP (10:1) Freeze-Dried Powder

Time(Month)	EE (%)		Size (nm)	PDI
	CU	PTX		
0	96.19 ± 4.16	94.79 ± 3.42	96.8 ± 0.5	0.174 ± 0.011
1	95.57 ± 1.03 <sup>#</sup>	94.98 ± 1.23 <sup>#</sup>	107.4 ± 0.7 <sup>#</sup>	0.167 ± 0.006 <sup>#</sup>
2	93.45 ± 4.40 <sup>#</sup>	94.46 ± 2.77 <sup>#</sup>	100.7 ± 0.7 <sup>#</sup>	0.146 ± 0.012 <sup>#</sup>
3	94.23 ± 0.42 <sup>#</sup>	93.49 ± 2.34 <sup>#</sup>	102.0 ± 3.5 <sup>#</sup>	0.164 ± 0.008 <sup>#</sup>

Note: <sup>#</sup>Compared with month 0, P >0.05.

death occurred at 0.5 h. Presumably, the extreme allergy and cardiotoxicity brought on by free PTX and the combined solvent (hydrogenated castor oil and anhydrous ethanol) caused this rapid death.<sup>52</sup> Within three days of the drug's treatment, all of the mice in the CU-PTX group passed away. The mice also showed decreased activity, decreased diet and water intake, decreased body weight, and hair loss. It is noteworthy that the presence of CU extends the time that mice survive relative to the PTX group. Only one mouse perished in the CU group on the third day following treatment, which may have been brought on by the use of mixed solvents. The mice in the CU-PTX-LNP, LNP, CU, and Control groups also exhibited normal dietary and water intake, mental state, and a modest rise in body weight.

As indicated in Table 10, the biochemical parameters of liver and kidney function assessed in the Control, LNP, CU, and CU-PTX-LNP groups fluctuated within the normal range. The AST of mice in the PTX and CU-PTX groups were higher than the normal reference range (60.0–220.0 U/L), with the PTX group's results being higher than the CU-PTX group's. Moreover, ALT in the PTX group exceeded the typical reference range (30.0–110.0 U/L). Elevated levels of

**Figure 8** Cumulative release rate (%) in vitro of CU and PTX for 96 h.



**Table 8** Model Fitting Results of CU-PTX-LNP

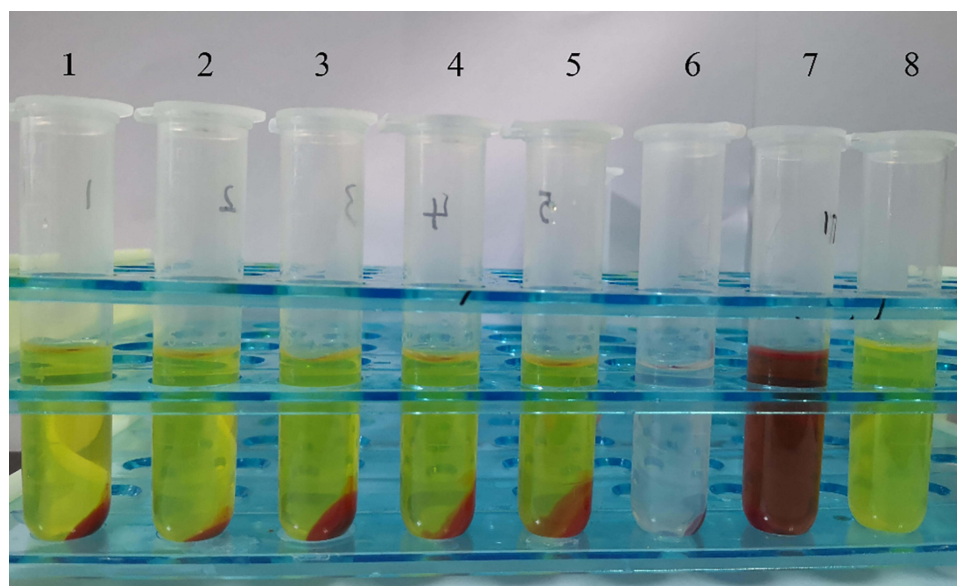
Release Model	CU		PTX	
	Equation	R	Equation	R
Zero-order equation	$M_t=0.56t + 6.44$	0.9362	$M_t=0.80t + 18.72$	0.8753
First-order equation	$M_t=56.71(1-e^{-0.03t})$	0.9258	$M_t=73.39(1-e^{-0.07t})$	0.8017
Higuchi equation	$M_t=5.70t^{1/2} - 1.24$	0.9756	$M_t=8.26t^{1/2} + 7.23$	0.9545

**Table 9** The Result of Hemolysis Testing of CU-PTX-LNP (2:1)

Number of the Test Tube	CU-PTX-LNP (2:1) (mL)	0.9% Saline (mL)	Ultrapure Water (mL)	2% Hematocyte (mL)	Hemolysis (%)
1	0.1	2.4	0	2.5	0.57±0.57
2	0.2	2.3	0	2.5	3.17±0.56
3	0.3	2.2	0	2.5	2.02±0.75
4	0.4	2.1	0	2.5	1.06±0.72
5	0.5	2.0	0	2.5	2.11±0.43
6	0	2.5	0	2.5	0.00
7	0	0	2.5	2.5	100.00
8	0.5	2.0	0	0	–

ALT and/or AST suggested decreased liver function in the PTX and CU-PTX groups, and the data suggested that the liver function abnormalities were more severe in the PTX group mice. These findings demonstrated that the liver's normal biochemical enzymology was disturbed.<sup>53</sup>

As shown in Figure 10, the heart, liver and kidney section images of mice in the Control, LNP and CU-PTX-LNP groups did not demonstrate pathological damage. The PTX group, CU-PTX group, and CU group showed localized strong eosinophilic changes in cardiomyocytes with blurred myofibrillar transverse lines and increased macrophages and mononuclear-like inflammatory cells. In contrast to the CU group, which showed no obvious injury, the PTX and CU-PTX groups of mice displayed enlarged renal tubular epithelial cells along with vacuolar degeneration and a slight

**Figure 9** The hemolysis of CU-PTX-LNP (2:1).

**Table 10** The Results of Liver and Kidney Function Tests ( $\bar{x} \pm s$ , n=3)

Parameters	Control	LNP	CU	PTX	CU-PTX	CU-PTX-LNP
ALP(U/L)	300.70±20.80	221.80±25.69	138.37±11.45	323.53±25.86	195.43±13.31	237.87±22.28
ALT(U/L)	57.00±17.72	46.30±1.98	44.15±5.55	117.50±23.84	48.13±3.31	74.23±16.07
AST(U/L)	142.07±35.44	102.27±13.78	189.8±18.77	591.13±74.88	375.93±47.13	153.30±20.54
CREA( $\mu$ mol/L)	18.27±3.72	15.53±2.10	28.03±3.63	27.93±7.96	21.70±1.69	24.80±3.11
UA( $\mu$ mol/L)	44.93±7.35	35.37±3.42	47.33±7.47	46.27±6.55	48.23±5.76	46.97±9.73
UREA(mmol/L)	7.28±0.40	7.03±0.84	7.22±0.15	19.25±2.98	9.93±0.35	9.71±0.43

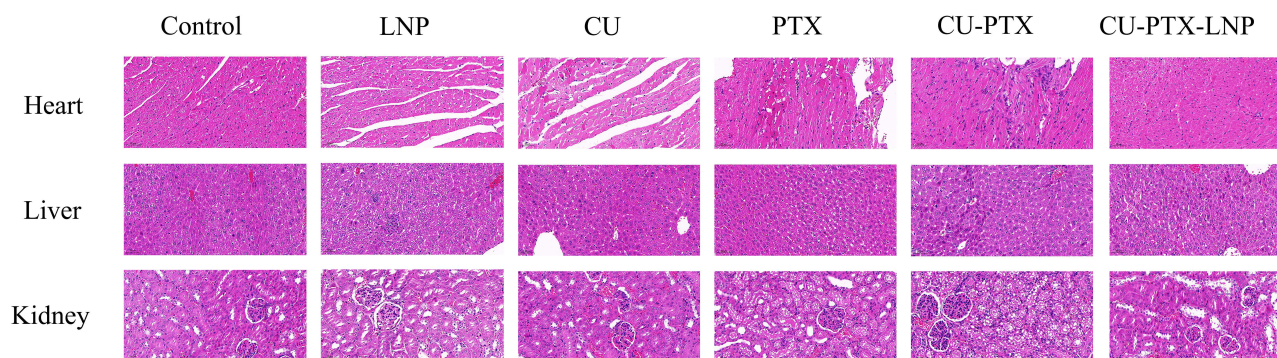
interstitial congestion in the kidney. Of interest, pictures of liver sections from mice in the PTX group showed enlarged hepatocytes with poor contour and increased Kupffer cells in the hepatic sinusoids. CU-PTX group showed a small number of hepatocytes with enhanced eosinophilia in the marginal zone of the hepatic lobules, whereas no significant injury was seen in the CU group. Usually, high doses of paclitaxel are closely associated with hepatotoxicity, nephrotoxicity and cardiotoxicity in preclinical studies and clinical settings,<sup>54–56</sup> and the use of mixed solvents may likewise lead to serious side effects,<sup>57,58</sup> including hypersensitivity reactions, nephrotoxicity, cardiotoxicity and neurotoxicity, which explains the cases of cardiac, hepatic and renal damage in the images of organ sections of mice in the PTX group, CU-PTX group and CU group. According to the findings of investigations on acute toxicity, both CU-PTX-LNP and blank LNP appear to have good safety profiles in mice.

## Pharmacokinetic Studies

The profiles of PTX and CU concentrations in plasma versus time are depicted in Figure 11. After 480 minutes of administration, free CU and PTX could not be detected while CU-PTX-LNP was detectable in plasma after 1440 minutes, clearly indicating that CU-PTX-LNP has a longer systemic circulation time. Pharmacokinetic parameters are presented in Table 11. CU-PTX-LNP exhibited higher MRT<sub>(0-t)</sub> (CU:4.13-fold, PTX:4.61-fold) and t<sub>1/2z</sub> (CU: 1.83-fold, PTX: 2.28-fold) compared with free CU-PTX. These results demonstrate that CU-PTX-LNP prolongs the retention times of active CU and PTX in vivo. On the one hand, the drugs can be protected from dilution, degradation or inactivation in circulation by incorporated into liposomes.<sup>46</sup> On the other hand, studies have found that pluronics modified liposomes exhibit enhanced stability and prolonged release behavior.<sup>47,48</sup> This may explain the extended MRT<sub>(0-t)</sub> and t<sub>1/2z</sub> of CU-PTX-LNP. Besides, plasma levels of CU showed lower Clearance rate (CLz) in CU-PTX-LNP, suggesting that the CU-PTX-LNP reduces CLz of CU, increasing MRT<sub>(0-t)</sub>, and thereby enhancing its absorption in vivo.

## In vivo Antitumor Investigation

The in vivo antitumor activity of CU-PTX-LNP was assessed by using nude mice bearing HepG2 tumor cells. The weight changes and tumor growth profiles of nude mice are shown in Figure 12 B and C, while the tumor weights and

**Figure 10** Histological sections of the heart, liver and kidney of KM mice treated with different drugs.

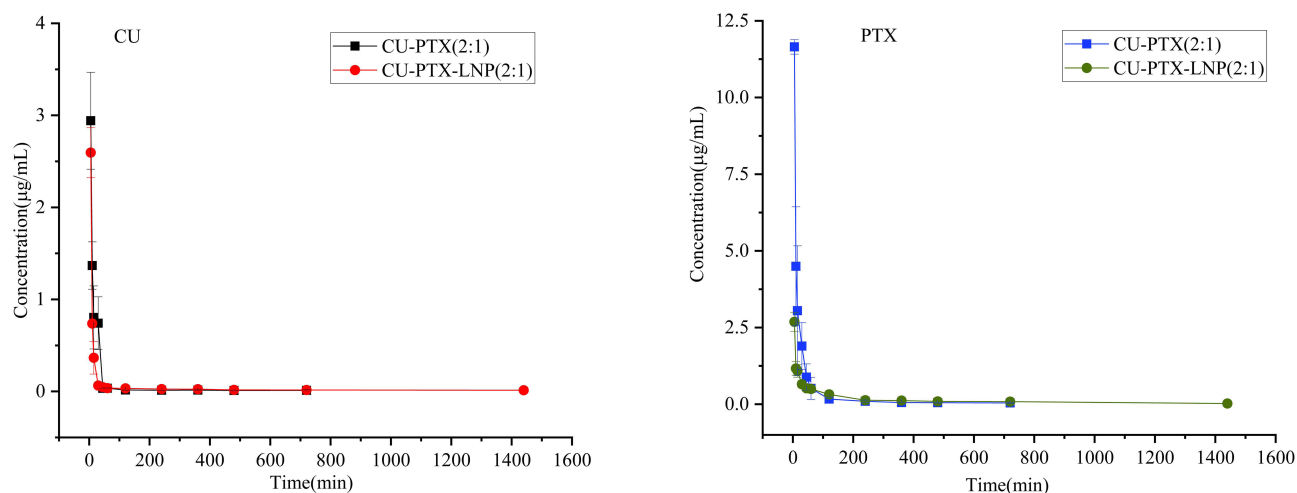


**Figure 11** The CU and PTX concentration curves of CU-PTX (2:1) and CU-PTX-LNP (2:1).

tumor photographs are shown in [Figure 12A](#) and [D](#). Throughout the experiment, PTX group and CU-PTX nude mice showed adverse manifestations such as decreased activity, reduced diet and water intake, and lethargy, while the nude mice in other groups were vigorous and behaved normally. The body weight of nude mice in the Control, CU, and CU-PTX-LNP groups did not change much and fluctuated within a certain range during the administration period, while it continuously decreased in the PTX and CU-PTX groups, indicating the use of PTX and mixed solvents (hydrogenated castor oil and anhydrous ethanol) caused clear side effects,<sup>59,60</sup> which was in line with the findings of acute toxicity experiments.

As shown in [Figure 12C](#), the tumor volume in the Control group increased rapidly during the experiment, especially the tumor growth rate accelerated rapidly after 7 days. In contrast, the CU group, PTX group, CU-PTX group, and CU-PTX-LNP group all showed limited tumor growth. In the later period, the CU-PTX combination group outperformed the PTX group in terms of slower tumor volume growth. Notably, the tumor volume growth was minimal in the CU-PTX-LNP administration group, which was consistent with the tumor suppression rate determined from the actual tumor weight at the conclusion of the trial. Specifically, the tumor suppression rates in each group were 26.78±8.49% (CU group); 51.33±3.56% (PTX group); 61.86±9.34% (CU-PTX group); and 64.18±6.42% (CU-PTX-LNP group). According to the aforementioned findings, CU can somewhat increase PTX's anti-hepatocellular carcinoma efficacy. And CU-PTX-LNP, which uses a biocompatible lipid platform as the drug carrier, exhibits potential efficacy. Besides, the CU-PTX-LNP group showed no significant side effects, indicating that it was safer than PTX and CU-PTX administered with mixed solvents and exhibited superior tumor growth inhibition at the same dose.

**Table 11** Pharmacokinetic Parameters of CU-PTX (2:1) and CU-PTX-LNP (2:1)

Parameter	Unit	CU-PTX (2: 1)		CU-PTX-LNP (2: 1)	
		CU	PTX	CU	PTX
AUC <sub>(0-t)</sub>	mg/L·min	64.216	271.689	64.048	199.689
MRT <sub>(0-t)</sub>	min	60.198	68.556	259.66	315.828
$t_{1/2z}$	min	673.859	207.159	1236.423	471.825
T <sub>max</sub>	min	5	5	5	5
V <sub>z</sub>	L/ kg	214.853	8.601	323.065	25.338
CL <sub>z</sub>	L/min/kg	0.221	0.029	0.181	0.037
C <sub>max</sub>	mg/L	2.9414	11.6507	2.5950	2.6851

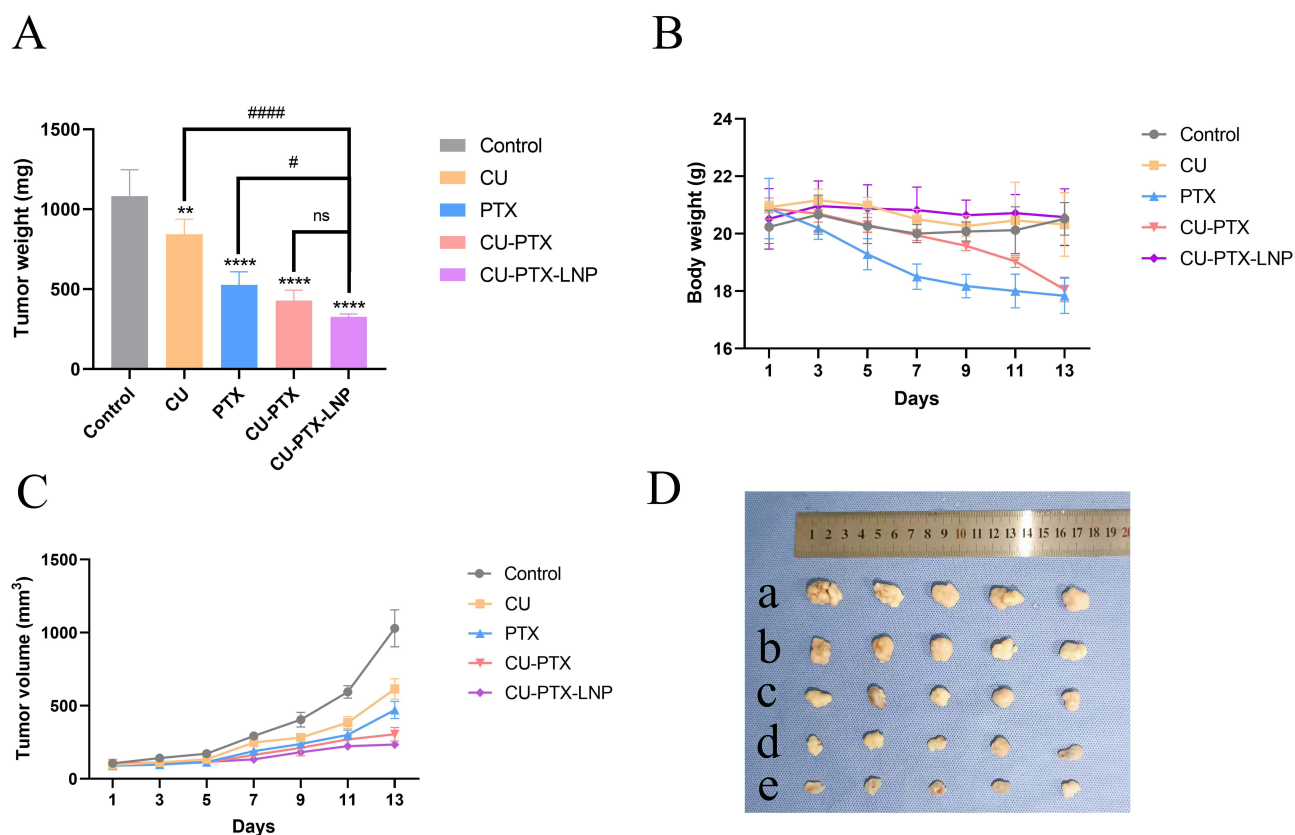


**Figure 12** In vivo antitumor activity of CU-PTX-LNP. **(A)** The weight of subcutaneous xenograft tumor in nude mice after 14 days. \*\* $P < 0.01$ , \*\*\*\* $P < 0.0001$ , compared with Control group; # $P < 0.05$ , ##### $P < 0.00001$ , compared with CU-PTX-LNP group. **(B)** Changes in body weight of nude mice. **(C)** Volume curve of subcutaneous xenograft tumor in nude mice. **(D)** Solid figure of subcutaneous xenograft tumor in nude mice. a, Control; b, CU; c, PTX; d, CU-PTX; e, CU-PTX-LNP.

## Conclusion

CU-PTX-LNP over a wide range of mass ratios was successfully constructed with high EE, ideal particle size, and PDI. Under the assumption of effective synergistic drug delivery, different ratios of the combined CU and PTX showed varying degrees of synergistic effects in the cytotoxicity assays. Additionally, CU-PTX-LNP demonstrated enhanced pharmacokinetics, good biosafety profile, and antitumor activity in vivo. In conclusion, development of CU-PTX-LNP as a general co-delivery platform provides a preliminary strategy to support the industrial production of an effective CU-PTX combined drug delivery system in the future.

## Abbreviations

CU, curcumin; PTX, paclitaxel; CU-LNP, curcumin lipid nanoplateform; CU-PTX-LNP, curcumin-paclitaxel lipid nanoplateform; DSC, differential scanning calorimetry; TEM, transmission electron microscope; XRD, X-ray diffraction; PDI, polydispersity index; MDR, multiple drug resistance; HSPC, hydrogenated soy phosphatidylcholine; PVP<sub>K15</sub>, polyvinylpyrrolidone; HPLC, high-performance liquid chromatography; EE, encapsulation efficiency.

## Acknowledgments

This study was supported by the central government guides the local science and technology development special fund (No.2022ZYD0084), the Major R&D Plan Joint Innovation Project (2022YFS0635, 2022YFS0630), the Youth Science and Technology Innovation Research Team (No. 2021JDTD0008) and the Basic Research fund (No. 2020YJ0336) of the Science and Technology Department of Sichuan province of China, the Science and Technology Innovation Team from Jiucheng Science and Technology Talent Cultivation Plan in Luzhou (No.2019-1), Key Research and Development Projectors of Luzhou (No. 2021-SYF-26), the cooperation Project (No. 210027-01SZ, 200017-01SZ) of Central Nervous System Drug Key



Laboratory of Sichuan Province, Chongqing Traditional Chinese Medicine Inheritance and Innovation Team Construction Project Traditional Chinese Medicine New Drug and Safety Research Inheritance and Innovation Team” (No.2022-8).

## Disclosure

The authors report no conflicts of interest in this work.

## References

1. Yang YH, Mao JW, Tan XL. Research progress on the source, production, and anti-cancer mechanisms of paclitaxel. *Chin J Nat Med.* 2020;18:890–897. doi:10.1016/S1875-5364(20)60032-2
2. Zhu L, Chen L. Progress in research on paclitaxel and tumor immunotherapy. *Cell Mol Biol Lett.* 2019;24:40. doi:10.1186/s11658-019-0164-y
3. Yu-Wei D, Li ZS, Xiong SM, et al. Paclitaxel induces apoptosis through the TAK1-JNK activation pathway. *FEBS Open Bio.* 2020;10:1655–1667. doi:10.1002/2211-5463.12917
4. Ren X, Zhao B, Chang H, Xiao M, Wu Y, Liu Y. Paclitaxel suppresses proliferation and induces apoptosis through regulation of ROS and the AKT/ MAPK signaling pathway in canine mammary gland tumor cells. *Mol Med Rep.* 2018;17:8289–8299. doi:10.3892/mmr.2018.8868
5. Zhang Y, Wang Y, Xue J. Paclitaxel inhibits breast cancer metastasis via suppression of Aurora kinase-mediated cofilin-1 activity. *Exp Ther Med.* 2018;15:1269–1276. doi:10.3892/etm.2017.5588
6. Dan VM, Raveendran RS, Baby S. Resistance to intervention: paclitaxel in breast cancer. *Mini Rev Med Chem.* 2021;21:1237–1268. doi:10.2174/1389557520999201214234421
7. Cui H, Arnst K, Miller DD, Li W. Recent advances in elucidating paclitaxel resistance mechanisms in non-small cell lung cancer and strategies to overcome drug resistance. *Curr Med Chem.* 2020;27:6573–6595. doi:10.2174/0929867326666191016113631
8. Maurer K, Michener C, Mahdi H, Rose PG. Universal tolerance of nab-paclitaxel for gynecologic malignancies in patients with prior taxane hypersensitivity reactions. *J Gynecol Oncol.* 2017;28:e38. doi:10.3802/jgo.2017.28.e38
9. Leskela S, Jara C, Leandro-Garcia LJ, et al. Polymorphisms in cytochromes P450 2C8 and 3A5 are associated with paclitaxel neurotoxicity. *Pharmacogenomics J.* 2011;11:121–129. doi:10.1038/tpj.2010.13
10. Malekinejad H, Ahsan S, Delkosh-Kasmaie F, Cheraghi H, Rezaei-Golmisheh A, Janbaz-Acyabar H. Cardioprotective effect of royal jelly on paclitaxel-induced cardio-toxicity in rats. *Iran J Basic Med Sci.* 2016;19:221–227.
11. Crown J, O’Leary M. The taxanes: an update. *Lancet.* 2000;355:1176–1178. doi:10.1016/S0140-6736(00)02074-2
12. Huang CY, Cheng M, Lee NR, et al. Comparing paclitaxel-carboplatin with paclitaxel-cisplatin as the front-line chemotherapy for patients with FIGO IIIC serous-type tubo-ovarian cancer. *Int J Environ Res Public Health.* 2020;17. doi:10.3390/ijerph17072213
13. Ezrahi S, Aserin A, Garti N. Basic principles of drug delivery systems - The case of paclitaxel. *Adv Colloid Interface Sci.* 2019;263:95–130. doi:10.1016/j.cis.2018.11.004
14. Feng X, Pi C, Fu S, et al. Combination of curcumin and paclitaxel liposomes exhibits enhanced cytotoxicity towards A549/A549-T cells and unaltered pharmacokinetics. *J Biomed Nanotechnol.* 2020;16:1304–1313. doi:10.1166/jbn.2020.2969
15. Wei Y, Pu X, Zhao L. Preclinical studies for the combination of paclitaxel and curcumin in cancer therapy (Review). *Oncol Rep.* 2017;37:3159–3166. doi:10.3892/or.2017.5593
16. Alemi A, Zavar Reza J, Haghirsadat F, et al. Paclitaxel and curcumin coadministration in novel cationic PEGylated niosomal formulations exhibit enhanced synergistic antitumor efficacy. *J Nanobiotechnology.* 2018;16:28. doi:10.1186/s12951-018-0351-4
17. Xu T, Guo P, He Y, et al. Application of curcumin and its derivatives in tumor multidrug resistance. *Phytother Res.* 2020;34:2438–2458. doi:10.1002/ptr.6694
18. Zheng B, McClements DJ. Formulation of more efficacious curcumin delivery systems using colloid science: enhanced solubility, stability, and bioavailability. *Molecules.* 2020;25:2791. doi:10.3390/molecules25122791
19. Tonnesen HH, Masson M, Loftsson T. Studies of curcumin and curcuminoids. XXVII. Cyclodextrin complexation: solubility, chemical and photochemical stability. *Int J Pharm.* 2002;244:127–135. doi:10.1016/s0378-5173(02)00323-x
20. Shen L, Liu CC, An CY, Ji HF. How does curcumin work with poor bioavailability? Clues from experimental and theoretical studies. *Sci Rep.* 2016;6:20872. doi:10.1038/srep20872
21. Kharat M, Du Z, Zhang G, McClements DJ. Physical and chemical stability of curcumin in aqueous solutions and emulsions: impact of pH, temperature, and molecular environment. *J Agric Food Chem.* 2017;65:1525–1532. doi:10.1021/acs.jafc.6b04815
22. Anand P, Kunnumakkara AB, Newman RA, Aggarwal BB. Bioavailability of curcumin: problems and promises. *Mol Pharm.* 2007;4:807–818. doi:10.1021/mp700113r
23. Zuo S, Wang Z, An X, et al. Self-assembly engineering nanodrugs composed of paclitaxel and curcumin for the combined treatment of triple negative breast cancer. *Front Bioeng Biotechnol.* 2021;9:747637. doi:10.3389/fbioe.2021.747637
24. Xiong K, Zhang Y, Wen Q, et al. Co-delivery of paclitaxel and curcumin by biodegradable polymeric nanoparticles for breast cancer chemotherapy. *Int J Pharm.* 2020;589:119875. doi:10.1016/j.ijpharm.2020.119875
25. Nguyen NT, Bui QA, Huynh PD, et al. Curcumin and paclitaxel co-loaded heparin and poloxamer p403 hybrid nanocarrier for improved synergistic efficacy in breast cancer. *Curr Drug Deliv.* 2022;19:966–979. doi:10.2174/1567201819666220401095923
26. Kim KR, You SJ, Kim HJ, et al. Theranostic potential of biodegradable polymeric nanoparticles with paclitaxel and curcumin against breast carcinoma. *Biomater Sci.* 2021;9:3750–3761. doi:10.1039/d1bm00370d
27. Anirudhan TS, Varghese S, Manjusha V. Hyaluronic acid coated Pluronic F127/Pluronic P123 mixed micelle for targeted delivery of paclitaxel and curcumin. *Int J Biol Macromol.* 2021;192:950–957. doi:10.1016/j.ijbiomac.2021.10.061
28. Xiong W, Qi L, Jiang N, et al. Metformin liposome-mediated PD-L1 downregulation for amplifying the photodynamic immunotherapy efficacy. *ACS Appl Mater Interfaces.* 2021;13:8026–8041. doi:10.1021/acsami.0c21743
29. Zhou Z, Chen J, Liu Y, et al. Cascade two-stage tumor re-oxygenation and immune re-sensitization mediated by self-assembled albumin-sorafenib nanoparticles for enhanced photodynamic immunotherapy. *Acta Pharm Sin B.* 2022;12:4204–4223. doi:10.1016/j.apsb.2022.07.023



30. Zhou Z, Liu Y, Song W, et al. Metabolic reprogramming mediated PD-L1 depression and hypoxia reversion to reactivate tumor therapy. *J Control Release*. 2022;352:793–812. doi:10.1016/j.jconrel.2022.11.004
31. Hasanpoor Z, Mostafaie A, Nikokar I, Hassan ZM. Curcumin-human serum albumin nanoparticles decorated with PDL1 binding peptide for targeting PDL1-expressing breast cancer cells. *Int J Biol Macromol*. 2020;159:137–153. doi:10.1016/j.ijbiomac.2020.04.130
32. Guan YY, Zeng SQ, Qin Y, Mu Y, Liu H. Vitamin E-tocopheryl polyethylene glycol succinate decorated drug delivery system with synergistic antitumor effects to reverse drug resistance and immunosuppression. *Colloids Surf A*. 2021;628. doi:10.1016/j.colsurfa.2021.127387
33. Jiang K, Shen M, Xu W. Arginine, glycine, aspartic acid peptide-modified paclitaxel and curcumin co-loaded liposome for the treatment of lung cancer: in vitro/vivo evaluation. *Int J Nanomedicine*. 2018;13:2561–2569. doi:10.2147/IJN.S157746
34. Gao J, Fan K, Jin Y, et al. PEGylated lipid bilayer coated mesoporous silica nanoparticles co-delivery of paclitaxel and curcumin leads to increased tumor site drug accumulation and reduced tumor burden. *Eur J Pharm Sci*. 2019;140:105070. doi:10.1016/j.ejps.2019.105070
35. Baek JS, Cho CW. A multifunctional lipid nanoparticle for co-delivery of paclitaxel and curcumin for targeted delivery and enhanced cytotoxicity in multidrug resistant breast cancer cells. *Oncotarget*. 2017;8:30369–30382. doi:10.18632/oncotarget.16153
36. Anwar M, Akhter S, Mallick N, et al. Enhanced anti-tumor efficacy of paclitaxel with PEGylated lipidic nanocapsules in presence of curcumin and poloxamer: in vitro and in vivo studies. *Pharmacol Res*. 2016;113:146–165. doi:10.1016/j.phrs.2016.08.025
37. Pi C, Zhao W, Zeng M, et al. Anti-lung cancer effect of paclitaxel solid lipid nanoparticles delivery system with curcumin as co-loading partner in vitro and in vivo. *Drug Deliv*. 2022;29:1878–1891. doi:10.1080/10717544.2022.2086938
38. Chou TC. Drug combination studies and their synergy quantification using the Chou-Talalay method. *Cancer Res*. 2010;70:440–446. doi:10.1158/0008-5472.CAN-09-1947
39. Padhi S, Kapoor R, Verma D, Panda AK, Iqbal Z. Formulation and optimization of topotecan nanoparticles: in vitro characterization, cytotoxicity, cellular uptake and pharmacokinetic outcomes. *J Photochem Photobiol B*. 2018;183:222–232. doi:10.1016/j.jphotobiol.2018.04.022
40. Win KY, Feng SS. Effects of particle size and surface coating on cellular uptake of polymeric nanoparticles for oral delivery of anticancer drugs. *Biomaterials*. 2005;26:2713–2722. doi:10.1016/j.biomaterials.2004.07.050
41. Gong X, Zheng Y, He G, Chen K, Zeng X, Chen Z. Multifunctional nanoplatform based on star-shaped copolymer for liver cancer targeting therapy. *Drug Deliv*. 2019;26:595–603. doi:10.1080/10717544.2019.1625467
42. Wang Y, Cui Y, Zhao Y, et al. Effects of surface modification and size on oral drug delivery of mesoporous silica formulation. *J Colloid Interface Sci*. 2018;513:736–747. doi:10.1016/j.jcis.2017.11.065
43. Kore G, Kolate A, Nej A, Misra A. Polymeric micelle as multifunctional pharmaceutical carriers. *J Nanosci Nanotechnol*. 2014;14:288–307. doi:10.1166/jnn.2014.9021
44. Banerjee A, Qi J, Gogoi R, Wong J, Mitragotri S. Role of nanoparticle size, shape and surface chemistry in oral drug delivery. *J Control Release*. 2016;238:176–185. doi:10.1016/j.jconrel.2016.07.051
45. Stylianopoulos T, Soteriou K, Fukumura D, Jain RK. Cationic nanoparticles have superior transvascular flux into solid tumors: insights from a mathematical model. *Ann Biomed Eng*. 2013;41:68–77. doi:10.1007/s10439-012-0630-4
46. Ruttala HB, Ko YT. Liposomal co-delivery of curcumin and albumin/paclitaxel nanoparticle for enhanced synergistic antitumor efficacy. *Colloids Surf B Biointerfaces*. 2015;128:419–426. doi:10.1016/j.colsurfb.2015.02.040
47. Davis ME, Chen ZG, Shin DM. Nanoparticle therapeutics: an emerging treatment modality for cancer. *Nat Rev Drug Discov*. 2008;7:771–782. doi:10.1038/nrd2614
48. Lal R, Ramachandran S, Arnsdorf MF. Multidimensional atomic force microscopy: a versatile novel technology for nanopharmacology research. *AAPS J*. 2010;12:716–728. doi:10.1208/s12248-010-9232-y
49. Beddoes CM, Case CP, Briscoe WH. Understanding nanoparticle cellular entry: a physicochemical perspective. *Adv Colloid Interface Sci*. 2015;218:48–68. doi:10.1016/j.cis.2015.01.007
50. Heger M, van Golen RF, Broekgaarden M, Michel MC. The molecular basis for the pharmacokinetics and pharmacodynamics of curcumin and its metabolites in relation to cancer. *Pharmacol Rev*. 2014;66:222–307. doi:10.1124/pr.110.004044
51. Xia Q, Ling L, Ismail M, et al. Paclitaxel encapsulated in artesunate-phospholipid liposomes for combinatorial delivery. *J Drug Deliv Sci Technol*. 2019;51:372–382. doi:10.1016/j.jddst.2019.03.010
52. Ashrafizadeh M, Zarrabi A, Hashemi F, et al. Curcumin in cancer therapy: a novel adjunct for combination chemotherapy with paclitaxel and alleviation of its adverse effects. *Life Sci*. 2020;256:117984. doi:10.1016/j.lfs.2020.117984
53. Wei Y, Zeng M, Pi C, et al. Novel curcumin derivative-decorated ultralong-circulating paclitaxel nanoparticles: a novel delivery system with superior anticancer efficacy and safety. *Int J Nanomedicine*. 2022;17:5265–5286. doi:10.2147/IJN.S369761
54. Ruger AM, Schneeweiss A, Seiler S, et al. Cardiotoxicity and cardiovascular biomarkers in patients with breast cancer: data from the GeparOcto-GBG 84 trial. *J Am Heart Assoc*. 2020;9:e018143. doi:10.1161/JAHA.120.018143
55. Gur C, Kandemir FM, Caglayan C, Satici E. Chemopreventive effects of hesperidin against paclitaxel-induced hepatotoxicity and nephrotoxicity via amendment of Nrf2/HO-1 and caspase-3/Bax/Bcl-2 signaling pathways. *Chem Biol Interact*. 2022;365:110073. doi:10.1016/j.cbi.2022.110073
56. Jeswani G, Chablani L, Gupta U, et al. Exploration of hemocompatibility and intratumoral accumulation of paclitaxel after loco-regional administration of thermoresponsive hydrogel composed of poloxamer and xanthan gum: an application to dose-dense chemotherapy. *Int J Biol Macromol*. 2023;226:746–759. doi:10.1016/j.ijbiomac.2022.11.285
57. Gradishar WJ, Tjulandin S, Davidson N, et al. Phase III trial of nanoparticle albumin-bound paclitaxel compared with polyethylated castor oil-based paclitaxel in women with breast cancer. *J Clin Oncol*. 2005;23:7794–7803. doi:10.1200/JCO.2005.04.937
58. Yoshizawa Y, Kono Y, Ogawara K, Kimura T, Higaki K. PEG liposomalization of paclitaxel improved its in vivo disposition and anti-tumor efficacy. *Int J Pharm*. 2011;412:132–141. doi:10.1016/j.ijpharm.2011.04.008
59. Xiong W, Peng L, Chen H, Li Q. Surface modification of MPEG-b-PCL-based nanoparticles via oxidative self-polymerization of dopamine for malignant melanoma therapy. *Int J Nanomedicine*. 2015;10:2985–2996. doi:10.2147/IJN.S79605
60. Qian J, Xu N, Zhou X, et al. Low density lipoprotein mimic nanoparticles composed of amphipathic hybrid peptides and lipids for tumor-targeted delivery of paclitaxel. *Int J Nanomedicine*. 2019;14:7431–7446. doi:10.2147/IJN.S215080

International Journal of Nanomedicine

Dovepress

### Publish your work in this journal

The International Journal of Nanomedicine is an international, peer-reviewed journal focusing on the application of nanotechnology in diagnostics, therapeutics, and drug delivery systems throughout the biomedical field. This journal is indexed on PubMed Central, MedLine, CAS, SciSearch<sup>®</sup>, Current Contents<sup>®</sup>/Clinical Medicine, Journal Citation Reports/Science Edition, EMBase, Scopus and the Elsevier Bibliographic databases. The manuscript management system is completely online and includes a very quick and fair peer-review system, which is all easy to use. Visit <http://www.dovepress.com/testimonials.php> to read real quotes from published authors.

Submit your manuscript here: <https://www.dovepress.com/international-journal-of-nanomedicine-journal>